PCCP

ROYAL SOCIETY OF CHEMISTRY

PAPER

View Article Online
View Journal | View Issue



Cite this: *Phys. Chem. Chem. Phys.*, 2026, **28**, 7476

# Mechanistic insight into the self-healing capability of solid-state lithium batteries: role of the PEO–$TiO_2$ interface

Federico Piciacchia, Sergio Tosoni * and Livia Giordano

Received 17th November 2025,
Accepted 17th February 2026

DOI: 10.1039/d5cp04444h

rsc.li/pccp

Lithium dendrite formation during cycling of solid-state lithium batteries (SSLB) is known to critically affect the duration of these devices, which limits their application, despite their promising overall performance. In this study, we performed a first-principles computational analysis of lithium interaction with anatase $TiO_2$ surfaces grafted with polyethylene oxide (PEO) – aiming at understanding the mechanism behind the self-healing behavior observed in batteries with composite electrolytes comprising nanoparticles of functionalized titania. We report a strong stabilization of Li species at the PEO/$TiO_2$ interface, which exposes several oxygen sites with good coordinative capability toward $Li^+$ cations, whose formation is enabled by the reducible nature of $TiO_2$, prone to host extra electrons in the empty Ti(3d) states. The role of PEO/$TiO_2$ nanostructures in dissolving dendrites, thus, may not be limited to a bare mechanical effect, as previously proposed, and also involves a chemical process of Li coordination and oxidation at the polymer/oxide interface.



## 1. Introduction

The future of energy storage lies in the battery's composition and most importantly in its energy storage efficiency. Nowadays, the main problem is to decouple the production of batteries from critical resources and to find more efficient, safe and sustainable materials. One of most promising formulations that is dominating the field is solid state batteries. Solid state lithium batteries (SSLBs) are a promising alternative to the liquid phase electrolyte batteries, which are known to suffer from safety issues and insufficient lifetime.[1,2] SSLBs are a macro-class of devices that can be divided into three subgroups: polymer-based, ceramic-based and hybrid, thus composed of a mixture of the aforementioned materials. On the one hand, ceramic materials have good mechanical and thermal resilience due to the covalent/ionic bonding nature, whereas polymers display plasticity and dynamic nature due to the weak interchain interactions. In the landscape of materials for batteries, polymers have recently been considered promising materials to improve batteries and move to new solutions for SSLBs. In particular, among many classes of polymers, polyethylene oxide(PEO) is one of the best candidates due to its flexibility, relative solubility and capacity to bind ions.

PEO-based SSLBs present outstanding qualities over other polymers due to their good affinity for Li salts, high flexibility, and favorable ionic conductivity.[3] Furthermore, in general, the formation of amorphous phases, where ions can easily diffuse, is easy in polymeric matrices, while it may be more complicated for other non-polymeric materials. Despite the promise of SSLBs in allowing the use of lithium metal anodes,[4] a severe issue affects their durability and cyclability: the formation of dendrites.[5] Indeed, while the battery is cycling, aggregations of lithium atoms of nanometric size can form at the surface of the Li electrode, eventually damaging the membrane and causing shortcuts and deactivation of the battery. At the base of dendrite formation stands a mechanism of lithium uneven deposition at the electrode/electrolyte interface, which triggers the growth of tree-like metallic protrusions.[6] These can form at the tip of the electrode, and then penetrate into the softer part of the membrane,[7,8] but also develop laterally on the electrode surface.[9] The surface morphology of the electrode,[10] the adhesion strength of the solid-state electrolyte at the electrode surface,[11] and phenomena of charge accumulation/depletion at the electrode/electrolyte interface may play an important role.[12,13] Although many attempts have been made to mitigate this problem, mostly by optimizing the physiochemical properties of the electrode/electrolyte interface, the formation of dendrites remains an open issue.[13] In addition, dendrite formation occurs for both ceramic and polymeric materials, because they propagate through the amorphous matrix in the polymer-based SSE and through grain borders in inorganic ceramic electrolytes.[14,15]

*Department of Materials Science, University of Milano-Bicocca, via Roberto Cozzi 55, Milan, Italy. E-mail: sergio.tosoni@unimib.it*

 

One of the most critical effects of lithium dendrite propagation is the piercing of the membrane, and consequently the loss of performance. Conditions to recover the operating conditions in SSLBs are the disaggregation of the dendrite induced mechanically by the polymer branches (razor effect), on one hand, and the recovery of the structural integrity in the membrane, on the other. Due to the dynamic nature of the polymer, its chains can spontaneously reassemble, giving rise to a phenomenon known as self-healing.[16,17] This property makes polymers potential substitutes for all those electronic components that undergo permanent mechanical and structural stress.[16,18] However, the bare mechanical action of the polymers on the dendrites may not be the only factor behind self-healing in SSLBs, and this is why interfacial phenomena in ceramic fillers functionalized with polymers are of high interest. In fact, membranes integrating ceramic and polymeric components show improved mechanical properties and enhanced chemical stability, as well as the aforementioned self-healing effect.[19] As discussed in a recent publication, composite polymer–inorganic solid electrolytes, composed of $TiO_2$ nanospheres, known for their good interaction with lithium, capped with polyethylene oxide (PEO) chains, can outperform all polymer solid state electrolytes (SSEs) in terms of durability and self-healing capability.[19] In particular, a peculiar behavior was observed, where the cells, after ceasing any operational capability due to shortcuts caused by dendrites, resumed their previous stripping–plating profiles, suggesting that what caused the shortcut had been dissolved.[19] This behavior was not noticed in pure PEO-derivative membranes, nor by bare titania nanoparticles, free of any surface functionalization, and was attributed to mechanically induced breaking of Li dendrites, which is called the ''razor effect''.[19] XPS and EPR spectra suggest that $TiO_2$ has a role in the $Li/Li^+$ oxidation.[19] Thus, behind the self-healing effect reported in L. Mezzomo *et al.*, there is also the intrinsic capability of a polymer to get back to its integrity once the dendrites have been mitigated. In this specific case, two levels of self-healing can therefore be identified: at the polymer level, where the structure of the membrane is regenerated and at the dendrite level, where the $TiO_2$ filler disrupts the dendrites. In this study, we will focus only on the chemical nature of the second mechanism. Since many of the interactions with dendrites and PEO/$TiO_2$ nanoparticles are not well characterized, insights from atomistic simulations on the interaction between lithium and solid electrolytes can provide useful information on the strategies to improve the SSLBs performances. The aim of this paper is to investigate the interaction of lithium with $TiO_2$ grafted with PEO, to infer whether the composite PEO/$TiO_2$ SSE is merely a steric or mechanical hindrance to the formation and propagation of dendrites, or the chemical stabilization of Li at the interface plays a role in the self-healing mechanism by providing a decomposition pathway for dendrites. The work is divided into two parts: the first one addresses what happens in proximity to the surface of grafted $TiO_2$; the second analyzes the interaction between PEO and Li. Indeed, since dendrites pierce and propagate through the membrane, lithium will get in contact with both the polymer and the oxide surface. The surface of the titania nanoparticles was modelled as anatase (101). We chose anatase since this is the most representative phase identified in ref. 19, and we then focused on its most stable (101) facet. We thus use the most stable plane exposed by anatase to model the nanoparticle surface. As for the polymer, the choice to truncate the chains to their first few units enables us to focus on the PEO/$TiO_2$ interfacial region. At the experimental working temperature of ref. 19, moreover, PEO is known to be amorphous.[19–22] One can thus exclude that long-range ordering effects will play a major role in stabilizing lithium ions between the polymer chains.

The grafting of PEO on the anatase surface was modeled by adsorbing a $-PO_3^{2-}$ terminated diglyme on an O-vacant anatase surface,[19] thus ensuring an overall neutral system, without the need to apply any charge correction. The phosphate/titania bonding region offers an oxygen-rich environment where Li can bind, with several non-equivalent sites.

## 2. Computational details

Spin-polarized density functional theory (DFT) calculations were performed using the code VASP 6.0 (Vienna Ab initio Simulation Package).[23,24] The interaction between cores and valence electrons was treated with the projector augmented wave (PAW) method.[25,26] H(1s), Li(2s), C(2s,2p), O(2s,2p), P(3s,3p), and Ti(4s,3d,4p) electrons were treated explicitly. The Perdew, Burke, and Ernzerhof (PBE) formulation of the exchange–correlation functional was adopted.[27] To account for the highly-correlated nature of Ti(3d) states, an effective ($U$–$J$) Hubbard parameter of 3 eV was added to penalize fractional occupation on cationic sites, as originally proposed by Dudarev *et al.* (PBE+$U$).[28] Long-range dispersion was accounted for semi-empirically by using the damped D3 correction.[29,30] The reciprocal space was sampled in the Γ point only, as justified by the large dimension of the supercell (*vide infra*).[31] A kinetic energy cutoff of 600 eV was used to truncate the expansion of the plane-wave basis set. Stopping criteria of $1 \times 10^{-6}$ eV (electronic loop) and $1 \times 10^{-2}$ eV Å$^{-1}$ (electronic loop) were adopted.

Starting from the relaxed anatase $TiO_2$ bulk, a (101) slab model was obtained using the SLABCUT routine in the CRYSTAL code.[32] $3 \times 3$ and $3 \times 6$ surface supercells were used to screen both single and double chain interactions. To graft the polymer in our model, we considered a phosphoester of diglyme adsorbing on an O-vacancy of $TiO_2$. The most favorable configuration of PEO on the $TiO_2$ surface was determined by means of static relaxations, starting from various possible covalent, and non-covalent binding modes. The density of polymer per cell is 0.83 chain nm$^{-2}$, while the chain–chain distance can vary from 1.04 nm to 1.18 nm for the single and double model, respectively. The slab thickness was limited to two layers to ensure reasonably fast calculations also for large supercells, one of which has been frozen to avoid computational burdens. In order to test the robustness of the model considering two layers, to lighten the computational cost,

inspection of the thickness has been done. A benchmark calculation regarding the thickness of the $TiO_2$ slab was performed with Hubbard correction ($U = 3$ eV), using the formation energy of an oxygen vacancy and the Li adsorption energy as test cases. For 2 layers, we obtained 4.62 eV and −1.65 for $E_{vac}$ and $E_{ads}$, respectively; analogously, for 3 layers we have 4.57 eV and −1.77 eV for $E_{vac}$ and $E_{ads}$, respectively (see SI, Tables S1 and S2 and Fig. S1). Thus, since both processes of vacancy and lithium adsorption remain reasonably with the same thermodynamics and almost the same values, these benchmarks allowed us to use the two-layer thick model for the rest of the study, according also to the literature for the vacancy formation energy.[33,34] A vacuum layer as thick as 17 Å, at least, is added in the supercell to avoid spurious interactions with the replica of the slab. The starting structures for anatase $TiO_2$ and Li bulk were downloaded from the AMCSD crystallographic database.[35]

### 2.1. Thermodynamic references for Li dendrites

The hypothetical stabilizing role of PEO/$TiO_2$ must be evaluated by considering the relative stability of Li atoms bound to PEO/$TiO_2$ with respect to thermodynamic reference states, mimicking the stability of the separated components. While for the membrane components, the choice of the reference states is trivial (either clean titania, PEO grafted on $TiO_2$, or free-standing PEO), for lithium the choice of the reference state is more complex. In fact, the self-healing process in the battery implies Li takeover by PEO/$TiO_2$ to dissolve the dendrites. These, however, display a highly non-trivial morphology related to the growth and ambient conditions (lithium concentration, electrochemical potential, steric factors, mechanical strain).[36,37] Given that it is not viable to include these factors in first-principle simulations, we here compare three ideal model structures as thermodynamic references for Li, in a process where a Li atom is ideally extracted from a dendrite to be bound at the $TiO_2$ surface, PEO/$TiO_2$ interface or PEO chains. In the first model, the thermodynamic reference is a Li atom in a surface lattice site of Li(100), the most stable surface of lithium; in this way, the lithium atom originates from the surface of a dendrite. Alternatively, one could consider the cost of creating a vacancy in lithium bulk as the energy price to pay for the dendrite dissolution. Finally, one may consider as a reference the cohesive energy per Li atom in Li bulk, thus envisaging the energy of Li in its thermodynamic most stable state as the reference, as usually done in *ab initio* thermodynamics.[37]

## 3. Results and discussion

### 3.1. Interaction of Li with the $TiO_2$ surface

We first discuss the interaction of lithium with the surface of $TiO_2$. The Li adsorption energy is described by the following equations, by considering a Li vacancy on the (100) surface (eqn (1)), in the bulk (eqn (2)) or bulk Li (eqn (3)) as the thermodynamic reference:

$$E_{ads} = E(TiO_{2\,surface} + Li) + E(Li_{surface\_vacancy}) - E(TiO_{2\ surface}) - E(Li_{surface}) \quad (1)$$

$$E_{ads} = E(TiO_{2\,surface} + Li) + E(Li_{bulk\_vacancy}) - E(TiO_{2\ surface}) - E(Li_{bulk}) \quad (2)$$

$$E_{ads} = E(TiO_{2\,surface} + Li) - E(TiO_{2\,surface}) - E(Li_{bulk/n}) \quad (3)$$

The adsorption energy of a lithium atom, calculated with respect to the three thermodynamic references, on the stoichiometric and oxygen-vacant anatase (101) surfaces is reported in Fig. 1. Negative values of $E_{ads}$ are obtained on both stoichiometric and oxygen-defective $TiO_2$, regardless of the chosen thermodynamic reference for Li. This implies that the stabilization of lithium species at the anatase surface is strong enough to compensate for the energy cost of extracting a Li atom from a perfect (100) surface, or from the bulk. This is relevant, since one can assume that complex dendritic structures will display many undercoordinated Li species, which should undergo an even more drastic stabilization when coordinated to $TiO_2$. Interestingly, $E_{ads}$ is larger on stoichiometric anatase compared to a defective $TiO_{2-x}$ model, in contrast to the commonly observed more reactive character of defective surfaces. This can be explained by the fact that Li, upon coordination on $TiO_2$, transfers one electron to the empty Ti(3d) orbitals, as proven by the spin density maps in Fig. 1.

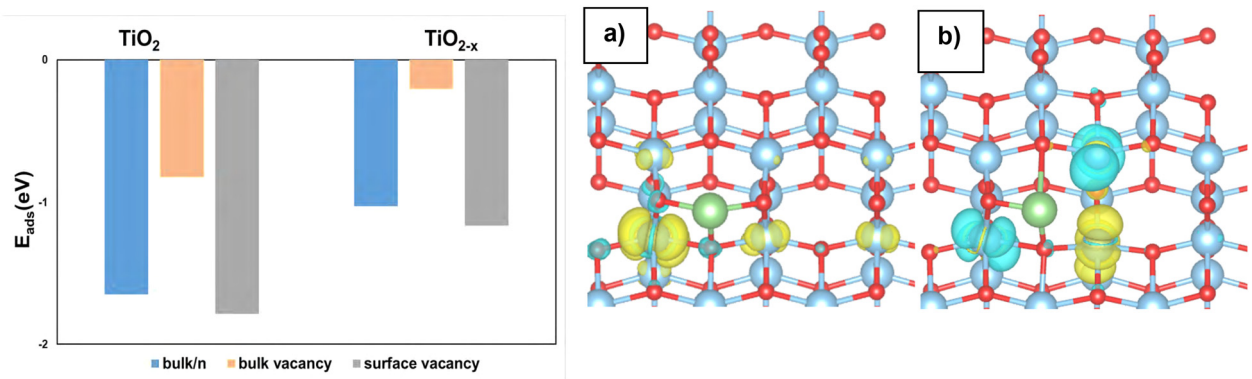


Fig. 1 Adsorption energy of Li on the anatase-$TiO_2$ (101) surface: stoichiometric (a) and O-vacant (b); Ti: cyan, O: red, Li: green. The spin density (isolevel of $5 \times 10^{-4}$|e| Å$^{-3}$) is displayed in yellow (up) and cyan (down) clouds.

 

In this respect, the presence of oxygen vacancies, which also contribute to populating Ti(3d) states, is detrimental. Moreover, a common trend is observed, where the adsorption energy calculated with respect to the formation of a surface vacancy in Li (eqn (1), grey column in Fig. 1) is more negative than that calculated with respect to the bulk cohesive energy (eqn (3), blue column in Fig. 1), which is in turn more negative than the one calculated with respect to a bulk Li vacancy (eqn (2), tangerine column in Fig. 1). The coherence of the results permits us to adopt the cohesive energy of Li in bulk, as in eqn (3), as a common reference in all calculations reported in the next Sections.

### 3.2. Interaction of Li at the PEO/$TiO_2$ interface

The adsorption of a single-Li atom was simulated at the PEO/$TiO_2$ interface on three different sites, mimicking a bridging of the $Li^+$ species between an oxygen ion from the phosphate binding group and a lattice oxygen ion from anatase (101).

Fig. 2 displays the relaxed structures along with the spin density. In site 1, Li is di-coordinated, bridging one O atom from the $TiO_2$ surface and one O atom from the phosphate terminating group. In site 2, a three-fold coordination of Li is envisaged (two O atoms from the phosphate group and one from $TiO_2$). Site 3 also displays a three-fold coordination, but Li is bound to two O from titania and only one from the polymer chain. In site 4, finally, Li is stabilized by the combined action of the titania surface and two PEO chains. The oxygen atoms from the phosphate group binding the PEO to the surface contribute remarkably to stabilizing the $Li^+$ species, with an increase in $E_{ads}$ (−2.32 eV on site 1, −1.82 eV on site 2 and −2.47 eV on site 3) with respect to bare $TiO_2$ (−1.66 eV). In all cases, the appearance of spin density on lattice Ti sites is clear evidence of the charge transfer from Li to $TiO_2$, in analogy with the case of bare titania (Fig. 1).

One may wonder, then, if a cooperative effect between several PEO chains in binding Li species is relevant. To conclude, we created a (3 × 4) supercell to accommodate two PEO chains, considering cross chain interaction and chain–chain–surface interaction. A new site originates from this model, site 4, as shown in Fig. 3 in which the coordination geometry of Li changes: in site 4, Li is chelated between the oxygen atoms of the ether groups in the diglyme units and the surface, with $E_{ads}$ (−2.51 eV) slightly more stable than the one obtained for the phosphate group binding to Li (site 2). Also, for this configuration, the spin density on surface Ti atoms indicates a charge transfer from Li to the oxide. The cooperative effect between PEO chains, thus, has little influence on the binding energy of a single Li ion. However, we cannot exclude that the chain–chain interaction will play a relevant role at a larger scale, where a dendrite approaches a functionalized nanoparticle.

It is worth noting that this larger model displays a density of grafting phosphates and reciprocal distances between the polymer chains comparable with the experimental results from ref. 19. According to the data reported in Fig. 3, the

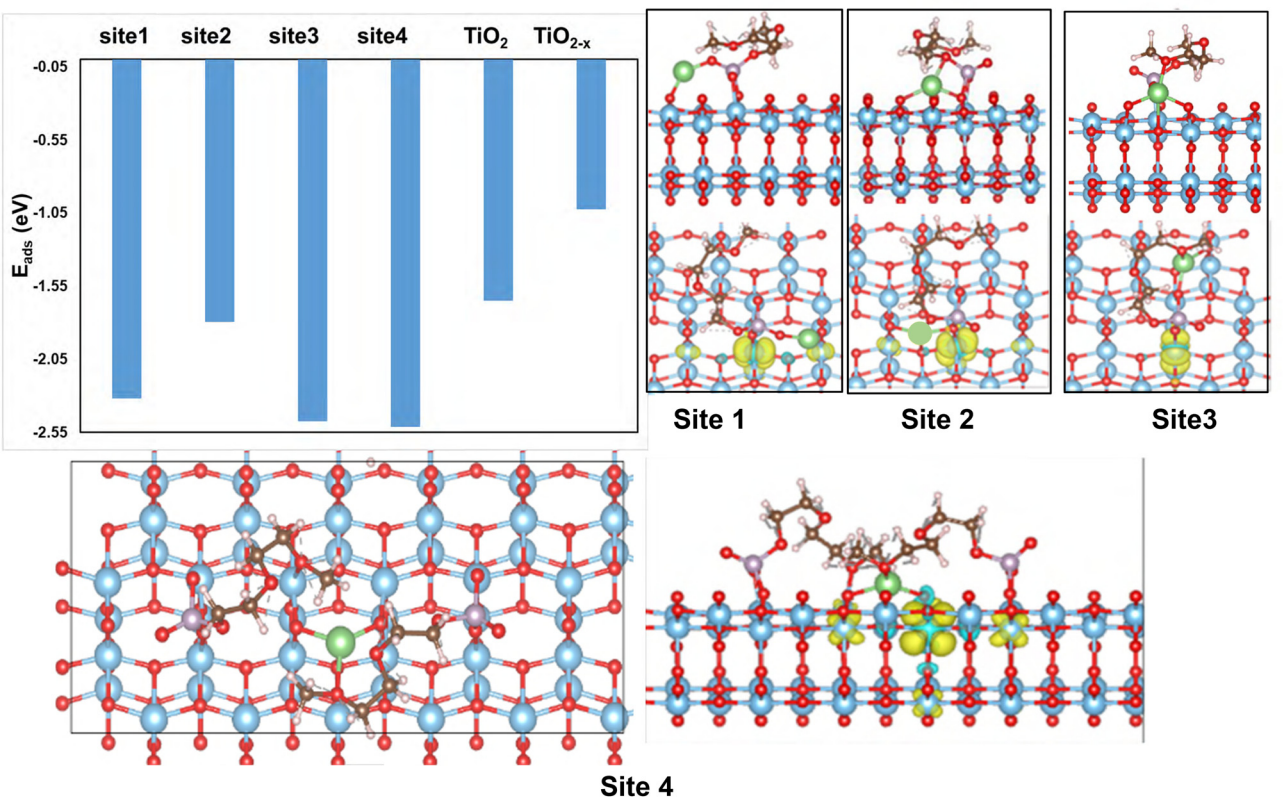


Fig. 2 Left: Adsorption energies of Li at different sites of PEO/$TIO_2$ interfaces, in comparison with bare $TiO_2$. Right: Top and side views of the structures with spin density (yellow clouds; isodensity = $5 \times 10^{-4}$|e| $Å^{-3}$). Ti: cyan, O: red, Li: green, P: grey, C: brown, and H: white.

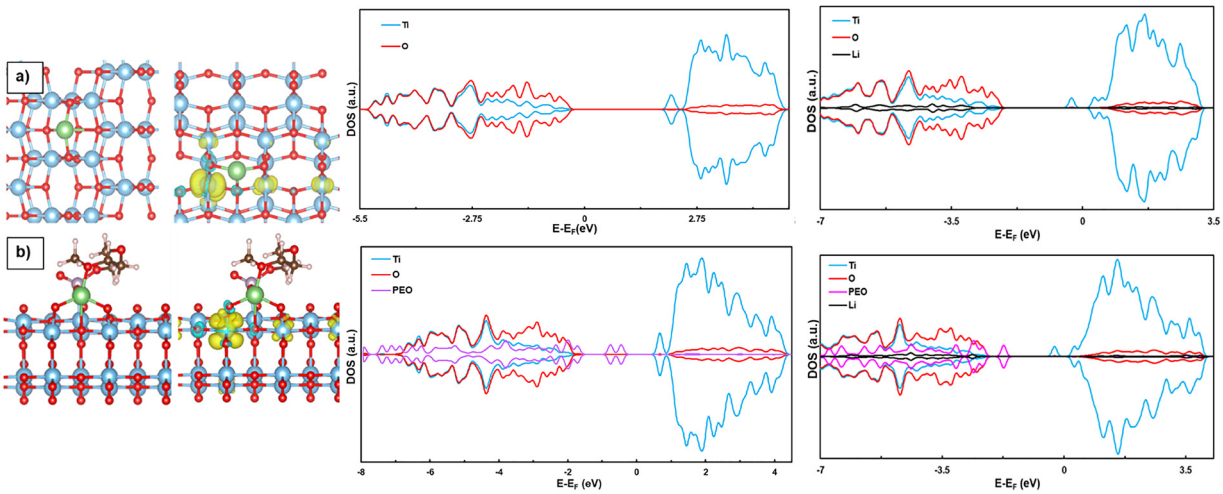


Fig. 3 Spin densities (yellow clouds; isodensity = $5 \times 10^{-4}|e|$ Å$^{-3}$) and PDOS of: (a) $TiO_2$ and Li@$TiO_2$; (b) PEO@$TiO_2$ and Li/PEO@$TiO_2$. Ti: cyan, O: red, Li: green, P: grey, C: brown, and H: white.

coordination of a Li atom between two PEO chains yields (in the most favorable case, site 4) a further slight stabilization (0.04 eV) compared to the best single-chain configuration (site 3, Fig. 2).

The projected density of states (PDOS) plots reported in Fig. 3a and b further confirm the electron donation from the Li(2s) orbital to Ti(3d) states, generating a shallow gap state centered on the metal 3d orbitals, upon binding of a Li atom to the anatase surface for both models. We now compare the adsorption properties of Li at the PEO@$TiO_2$ interface with those on pure PEO. It is worth mentioning that the grafting with the polymer generates surface states that can further accept electrons. For both models, anyway, it is found that the $Li^+$ electron is localized in the band below Fermi's level corresponding to 3d orbitals of Ti. However, with a semi-core alignment (SI) we could state that the nature of the process is mostly due to the coordination of the polymer with respect to the $Li^+$; in fact, the electron for $TiO_2$ and PEO@$TiO_2$ is localized in the same energy level, confirming that the nature is due to the presence of more basic oxygens belonging to the polymer, resulting in a less strained structure.

By considering a single PEO chain, Li coordinates with the oxygens of the polymer, as depicted in Fig. 4. The binding energy of Li to PEO is in this case +0.71 eV with respect to Li

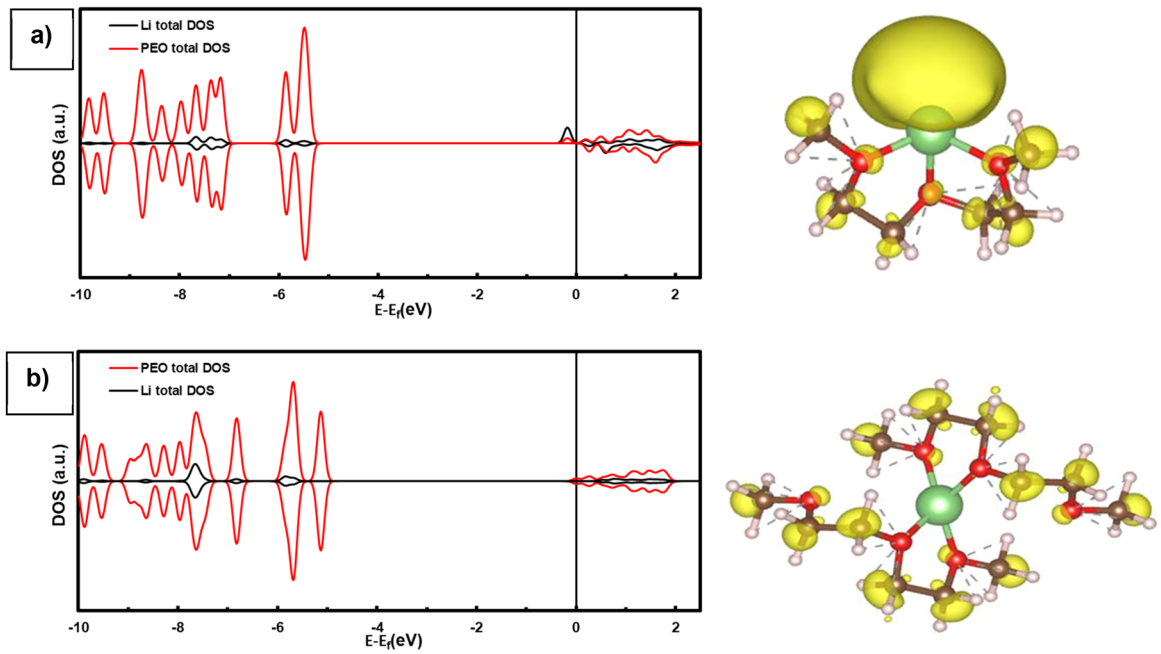


Fig. 4 PDOS of (a) Li@PEO diglyme with metallic Li near the Fermi level, (b) Li@$(PEO\ diglyme)_2$; the vertical black line represents the Fermi level. The corresponding structures are reported on the right: O: red, Li: green, C: brown, and H: white. The spin density is represented as yellow clouds (isodensity = $5 \times 10^{-4}|e|$ Å$^{-3}$).

 

bulk, indicating that PEO diglyme alone cannot cause the detachment of Li atomic species for dendrites, at variance from what is observed for $TiO_2$ (101) and PEO/$TiO_2$. Moreover, the DOS plot for a Li atom is bound to a free-standing PEO chain (Fig. 4a) indicating that the Li atom retains its neutral $2s^1$ electron configuration, and no electron transfer to PEO takes place, as also shown by the spin density.

Considering that in the real system free-standing PEO forms amorphous polymeric networks, Li species could find a more favorable oxygen-rich environment with respect to the model with a limited number of Li–O interactions discussed above. According to coordination of Li by PEO found in the literature,[38] a two-chain PEO model has been considered (Fig. 4). The spin density and DOS of a Li@$(PEO)_2$ model are represented in Fig. 4b, where two chains of polymer bind a Li atom in a tetrahedral geometry between four oxygen atoms, instead of a coordination number equal to 3, like in the single-chain model.

The DOS plot reveals a neat peak in the valence of the $(PEO)_2$ complex, indicating that the charge transfer partially occurred, even though a partial charge transfer from Li on the LUMO acceptor states (mostly centered on C atoms) of the polymer is evident from the spin density in Fig. 4. The computed Bader charge[39,40] reveals a substantial oxidation of Li (+0.87|$e$|).

The binding energy calculated for this model is small and positive (+0.25 eV), which means that the coordinated action of two PEO chains in chelating a Li species is stronger compared to bonding to a single chain, but much less favorable even than $TiO_2$ without any functionalization. Slightly more favorable binding energies for Li in amorphous PEO were previously reported in the literature.[38] This can be explained considering the difference between the two structural models, a periodic model mimicking an amorphous polymer *versus* a molecular model, and it may be due to the high structural flexibility of the long polymeric chains, which allows for a favorable coordination of Li species.

Finally, all the energies reported here were calculated at 0 K, but the inclusion of the thermal contribution at 343.15 K (working temperature of this type of battery) does not change the picture substantially, since the correspondent value of 343.15 K in electronvolt is 0.03, and this is not enough to change the adsorption profile and make it favorable for only PEO to chelate the Li atom and accept its electron.

## 4. Conclusions

In conclusion, it is possible to claim that the dendrite dissolution at the base of the experimentally observed electrochemical cell self-healing may be due to several factors, spanning from a mechanical-grounded razor effect of the polymeric chain on the dendrites (not discussed in this paper) to a more chemically based phenomenon, which was here treated in depth by means of DFT calculations: a redox process favorably oxidizing Li species, thanks to the reducible nature of titania. In this respect, the PEO/$TiO_2$ interface is expected to play a two-fold role: on the one hand, it enhances the stabilization of Li species at the polymer–oxide interface, thanks to the coordinative capability of the grafted phosphate groups towards $Li^+$ ions formed by the electron transfer to Ti-3d states, while, on the other, it could facilitate the transport of dispersed Li species to their stable binding sites. The presence of oxygen vacancies in $TiO_2$ is detrimental for the stabilization of ionized lithium, due to the competing reduction of the titania support, but stable binding of $Li^+$ is possible also on defective $TiO_2$. Conversely, free-standing PEO is scarcely able to bind and oxidize neutral lithium species. Notably, the favorable thermodynamic profile of Li adsorption on PEO/$TiO_2$ is obtained with respect to a Li atom in the bulk as a reference, which underlines the strong thermodynamic drive toward dissolution of dendritic lithium structures, which can be assumed to be less stable than the perfect Li bulk.

## Conflicts of interest

The authors have no conflicts of interest to declare.

## Data availability

The data supporting this article have been included as part of the supplementary information (SI). Supplementary information includes supporting data concerning oxygen vacancy formation and Li adsorption, to validate the adopted computational methodology. See DOI: https://doi.org/10.1039/d5cp04444h.

## Acknowledgements

The authors acknowledge funding from the ORANGEES project (Italian Ministry of Environment and Energy Security, Research of the National Electric System PTR 2019–2021). Financial support from ICSC – Centro Nazionale di Ricerca in High Performance Computing, Big Data and Quantum Computing, funded by European Union – NextGenerationEU, is also acknowledged. Access to CINECA supercomputing resources was granted *via* ISCRA-B.

## References

1 B. Łukasz, I. Rybakowska, A. Krakowiak, M. Gregorczyk and W. Waldman, Lithium batteries safety, wider perspective, *Int. J. Occup. Med. Environ. Health*, 2023, **36**, 3–20.
2 L. Xu, S. Tang, Y. Cheng, K. Wang, J. Liang, C. Liu, Y.-C. Cao, F. Wei and L. Mai, Interfaces in Solid-State Lithium Batteries, *Joule*, 2018, **2**, 1991–2015.
3 B. Guo, Y. Fu, J. Wang, Y. Gong, Y. Zhao, K. Yang, S. Zhou, L. Liu, S. Yang, X. Liu and F. Pan, Strategies and characterization methods for achieving high performance PEO-based solid-state lithium-ion batteries, *Chem. Commun.*, 2022, **58**, 8182–8193.
4 S. Randau, D. A. Weber, O. Kötz, R. Koerver, P. Braun, A. Weber, E. Ivers-Tiffée, T. Adermann, J. Kulisch,

W. G. Zeier, F. H. Richter and J. Janek, Benchmarking the performance of all-solid-state lithium batteries, *Nat. Energy*, 2020, **5**, 259–270.

5 Y. Guo, S. Wu, Y.-B. He, F. Kang, L. Chen, H. Li and Q.-H. Yang, Solid-state lithium batteries: Safety and prospects, *eScience*, 2022, **2**, 138–163.

6 M. Sun, T. Liu, Y. Yuan, M. Ling, N. Xu, Y. Liu, L. Yan, H. Li, C. Liu, Y. Lu, Y. Shi, Y. He, Y. Guo, X. Tao, C. Liang and J. Lu, Visualizing Lithium Dendrite Formation within Solid-State Electrolytes, *ACS Energy Lett.*, 2021, **6**, 451–458.

7 C. Brissot, M. Rosso, J.-N. Chazalviel and S. Lascaud, Dendritic growth mechanisms in lithium/polymer cells, *J. Power Sources*, 1999, **81–82**, 925–929.

8 J. L. Barton and J. O. Bockris, The electrolytic growth of dendrites from ionic solutions, *Proc. R. Soc. London, Ser. A*, 1962, **268**, 485–505.

9 M. Dollé, L. Sannier, B. Beaudoin, M. Trentin and J.-M. Tarascon, Live Scanning Electron Microscope Observations of Dendritic Growth in Lithium/Polymer Cells, *Electrochem. Solid-State Lett.*, 2002, **5**, A286.

10 K. J. Harry, D. T. Hallinan, D. Y. Parkinson, A. A. MacDowell and N. P. Balsara, Detection of subsurface structures underneath dendrites formed on cycled lithium metal electrodes, *Nat. Mater.*, 2014, **13**, 69–73.

11 X.-B. Cheng, C.-Z. Zhao, Y.-X. Yao, H. Liu and Q. Zhang, Recent Advances in Energy Chemistry between Solid-State Electrolyte and Safe Lithium-Metal Anodes, *Chemistry*, 2019, **5**, 74–96.

12 C.-Z. Zhao, P.-Y. Chen, R. Zhang, X. Chen, B.-Q. Li, X.-Q. Zhang, X.-B. Cheng and Q. Zhang, An ion redistributor for dendrite-free lithium metal anodes, *Sci. Adv.*, 2018, **4**(11), eaat3446.

13 J.-N. Chazalviel, Electrochemical aspects of the generation of ramified metallic electrodeposits, *Phys. Rev. A*, 1990, **42**, 7355–7367.

14 G. Bieker, M. Winter and P. Bieker, Electrochemical in situ investigations of SEI and dendrite formation on the lithium metal anode, *Phys. Chem. Chem. Phys.*, 2015, **17**, 8670–8679.

15 J. Becherer, D. Kramer and R. Mönig, Similarities in Lithium Growth at Vastly Different Rates, *ChemElectroChem*, 2021, **8**, 3882–3893.

16 J. Dahlke, S. Zechel, M. D. Hager and U. S. Schubert, How to Design a Self-Healing Polymer: General Concepts of Dynamic Covalent Bonds and Their Application for Intrinsic Healable Materials, *Adv. Mater. Interfaces*, 2018, **5**(17), 1800051.

17 J. Wang, G. Zhu, Y. Jia, L. Wang, J. Luo and S. Liu, The In Situ Polyelectrolyte With Liquid Metal Filler for High Rate and High Stability Quasi-Solid-State Sodium Battery, *Adv. Funct. Mater.*, 2025, **35**(43), 2505197.

18 F. Chen, H. Huang, W. Chen, H. Wu, T. Zou, X. Zhang, Y. Huang and X. Ding, Self-Adaptive Polymer Electrolytes for Lithium-Ion Batteries: Advances and Prospects, *ACS Appl. Energy Mater.*, 2025, **8**, 10007–10036.

19 L. Mezzomo, R. Lorenzi, M. Mauri, R. Simonutti, M. D'Arienzo, T. U. Wi, S. Ko, H. W. Lee, L. Poggini, A. Caneschi, P. Mustarelli and R. Ruffo, Unveiling the Role of PEO-Capped $TiO_2$ Nanofiller in Stabilizing the Anode Interface in Lithium Metal Batteries, *Nano Lett.*, 2022, **22**, 8509–8518.

20 S. Jagannathan, A. Shanmuga Sundaram, V. Kanchana and R. Rajesh, Thermal Property Analysis and Characteristic Study of Ploy Ethylene Glycol with Diverse Molecular Weight for Thermal Energy Storage Material, *IOP Conf. Ser.: Mater. Sci. Eng.*, 2020, **988**, 012081.

21 S. Yang, Z. Liu, Y. Liu and Y. Jiao, Effect of molecular weight on conformational changes of PEO: an infrared spectroscopic analysis, *J. Mater. Sci.*, 2015, **50**, 1544–1552.

22 B. K. Money and J. Swenson, Dynamics of poly(ethylene oxide) around its melting temperature, *Macromolecules*, 2013, **46**, 6949–6954.

23 G. Kresse and J. Furthmüller, Efficiency of ab-initio total energy calculations for metals and semiconductors using a plane-wave basis set, *Comput. Mater. Sci.*, 1996, **6**, 15–50.

24 G. Kresse and J. Furthmüller, Efficient iterative schemes for *ab initio* total-energy calculations using a plane-wave basis set, *Phys. Rev. B: Condens. Matter Mater. Phys.*, 1996, **54**, 11169–11186.

25 P. E. Blöchl, Projector augmented-wave method, *Phys. Rev. B: Condens. Matter Mater. Phys.*, 1994, **50**, 17953–17979.

26 G. Kresse and D. Joubert, From ultrasoft pseudopotentials to the projector augmented-wave method, *Phys. Rev. B: Condens. Matter Mater. Phys.*, 1999, **59**, 1758–1775.

27 J. P. Perdew, K. Burke and M. Ernzerhof, Generalized Gradient Approximation Made Simple, *Phys. Rev. Lett.*, 1996, **77**, 3865–3868.

28 K. Park, M. Raman, A. J. Olatunbosun and J. Pohlmann, Revisiting DFT+U calculations of $TiO_2$ and the effect of the local-projection size, *AIP Adv.*, 2024, **14**(6), 065114.

29 S. Grimme, J. Antony, S. Ehrlich and H. Krieg, A consistent and accurate ab initio parametrization of density functional dispersion correction (DFT-D) for the 94 elements H-Pu, *J. Chem. Phys.*, 2010, **132**, 154104.

30 S. Grimme, S. Ehrlich and L. Goerigk, Effect of the damping function in dispersion corrected density functional theory, *J. Comput. Chem.*, 2011, **32**, 1456–1465.

31 H. J. Monkhorst and J. D. Pack, Special points for Brillouin-zone integrations, *Phys. Rev. B: Solid State*, 1976, **13**, 5188–5192.

32 R. Dovesi, R. Orlando, A. Erba, C. M. Zicovich-Wilson, B. Civalleri, S. Casassa, L. Maschio, M. Ferrabone, M. De La Pierre, P. D'Arco, Y. Noël, M. Causà, M. Rérat and B. Kirtman, $C_{RYSTAL14}$: A program for the ab initio investigation of crystalline solids, *Int. J. Quantum Chem.*, 2014, **114**, 1287–1317.

33 A. N. Alexandrova and J. M.-A. Ha, Oxygen Vacancies of Anatase(101): Extreme Sensitivity to the Density Functional Theory Method, *Chem. Theory Comput.*, 2016, 2889–2895.

34 G. Mattioli, F. Filippone, P. Alippi and A. Amore Bonapasta, *Ab initio* study of the electronic states induced by oxygen vacancies in rutile and anatase $TiO_2$, *Phys. Rev. B: Condens. Matter Mater. Phys.*, 2008, **78**, 241201.

 

35 M. Hall-Wallace and R. T. Downs, The American Mineralogist Crystal Structure Database, *Am. Mineral.*, 2003, **88**, 247–250.
36 W. Mu, X. Liu, Z. Wen and L. Liu, Numerical simulation of the factors affecting the growth of lithium dendrites, *J. Energy Storage*, 2019, **26**, 100921.
37 A. Jana, S. I. Woo, K. S. N. Vikrant and R. E. García, Electrochemomechanics of lithium dendrite growth, *Energy Environ. Sci.*, 2019, **12**, 3595–3607.
38 D. Das, A. Chandrasekaran, S. Venkatram and R. Ramprasad, Effect of Crystallinity on Li Adsorption in Polyethylene Oxide, *Chem. Mater.*, 2018, **30**, 8804–8810.
39 R. F. W. Bader, A Quantum Theory of Molecular Structure and Its Applications, *Chem. Rev.*, 1991, **91**, 893–928.
40 G. Henkelman, A. Arnaldsson and H. Jónsson, A fast and robust algorithm for Bader decomposition of charge density, *Comput. Mater. Sci.*, 2006, **36**, 354–360.